ApJ, in press
Preprint typeset using LaTeX style emulateapj v. 6/22/04

INTEGRATED NEBULAR ABUNDANCES OF DISK GALAXIES

John Moustakas[1] & Robert C. Kennicutt, Jr.[1,2]

ApJ, in press

ABSTRACT

We study whether integrated optical spectroscopy of a disk galaxy can be used to infer the mean, or characteristic gas-phase oxygen abundance in the presence of systematic effects such as spatial abundance variations, contributions to the integrated emission-line spectrum from diffuse-ionized gas, and dust attenuation. Our sample consists of 14 nearby disk galaxies with integrated spectrophotometry, and observations of more than 250 individual H II regions culled from the literature. We consider both theoretical and empirical strong-line abundance calibrations based on the $R_{23} \equiv ([\mathrm{O\ II}] + [\mathrm{O\ III}])/\mathrm{H}\beta$ parameter. We find that the integrated oxygen abundance correlates well with the gas-phase abundance measured at a fixed galactocentric radius, as determined by the H II-region abundance gradient. The typical scatter in the correlation is ± 0.1 dex, independent of the abundance calibration, or whether the observed integrated emission-line fluxes, the reddening-corrected fluxes, or the emission-line equivalent widths are used. Integrated abundances based on the observed fluxes or equivalent widths, however, are susceptible to additional systematic effects of order $0.05 - 0.1$ dex, at least for the range of reddenings and stellar populations spanned by our sample. Unlike the integrated R_{23} parameter, we find that the integrated [N II]/Hα and [S II]/Hα ratios are enhanced with respect to line-ratios typical of H II regions, consistent with a modest contribution from diffuse-ionized gas emission. We conclude that the R_{23} parameter can be used to reliably measure the gas-phase abundances of distant star-forming galaxies.

Subject headings: galaxies: abundances — galaxies: evolution — galaxies: spiral

1. INTRODUCTION

Improving constraints on the chemical evolution histories of star-forming galaxies requires abundance measurements with well-understood systematic uncertainties. Quantifying these uncertainties is particularly important in light of recent results which show that typical star-forming galaxies undergo a relatively modest amount of chemical enrichment since $z \sim 1$ (J. Moustakas et al. 2006, in preparation; Lilly et al. 2003; Maier et al. 2004; Kobulnicky et al. 2003; Kobulnicky & Kewley 2004; Savaglio et al. 2005).

In the nearby universe, galaxies are resolved into individual H II regions, enabling a direct measurement of the gas-phase abundance at discreet spatial positions. By comparison, spectra of distant galaxies are a luminosity-weighted average of star-forming regions spanning a range of physical conditions, stars, and diffuse gas. In this paper we investigate whether spatially unresolved spectroscopy of spiral galaxies encompassing all, or a significant fraction of the light, reliably measures the gas-phase abundance as determined from spectroscopy of individual H II regions.

Our analysis focuses on disk galaxies for two reasons. First, luminous star-forming disk galaxies at high redshift are more likely to be observed compared to low-luminosity dwarf galaxies. Second, several physical properties of disk galaxies may systematically bias abundance measurements based on integrated spectroscopy. For example, whereas spiral galaxies exhibit radial abundance variations, to first order, dwarf galaxies are chemically homogenous (e.g., Kobulnicky & Skillman 1996). Therefore, we anticipate the largest discrepancy between integrated and spatially resolved abundances to arise in a sample of disk galaxies.

One of the most striking and characteristic properties of disk galaxies is the tendency for their centers to be more metal rich than their outskirts. Although the exact physical processes that give rise to radial abundance gradients are still a matter of debate (Molla et al. 1996, and references therein), it has been shown that the vast majority of nearby disk galaxies, if not all, possess radial gradients (e.g., Vila-Costas & Edmunds 1992; Zaritsky et al. 1994; van Zee et al. 1998). Since distant galaxies may have steeper abundance gradients, indicative of their earlier evolutionary state (e.g., Molla et al. 1997), it is important to quantify how variations in the slope of the abundance gradient affects the abundances we infer from integrated spectroscopy.

Another common, if not ubiquitous physical property of spiral galaxies, including the Milky Way, is the diffuse, low surface-brightness phase of the interstellar medium called the diffuse-ionized gas (DIG), or the diffuse-ionized medium (e.g., Reynolds 1990; Haffner et al. 1999; Ferguson et al. 1996; Wang et al. 1997; Greenawalt et al. 1998; Zurita et al. 2000; Thilker et al. 2002). Of order $30 - 50\%$ of the integrated Hα luminosity in spiral galaxies can be attributed to the DIG, making it an energetically important component of the interstellar medium of disk galaxies (Calzetti et al. 2004, and references therein). Since low-ionization line-ratios such as [N II]/Hα and [S II]/Hα in the DIG are enhanced relative to ratios involving high-excitation lines such as [O III]/Hβ (e.g., Martin 1997; Hoopes & Walterbos 2003), we want to determine what effect, if any, the integrated DIG emission of a disk galaxy has on the abundance we measure

[1] Steward Observatory, University of Arizona, 933 N Cherry Ave., Tucson, AZ 85721, USA; jmoustakas@as.arizona.edu
[2] Institute of Astronomy, University of Cambridge, Madingley Road, Cambridge CB3 0HA, UK; robk@ast.cam.ac.uk

from its integrated spectrum.

Finally, it is important to explore how variations in dust attenuation might bias integrated abundance measurements. Since the Hα line becomes inaccessible to ground-based optical spectroscopy above $z \approx 0.4$, it may not always be possible to correct the nebular lines for dust reddening (e.g., Kobulnicky et al. 2003, but see, e.g., Liang et al. 2004 and Maier et al. 2005). Therefore, we compare the abundances derived from the observed line fluxes, the reddening-corrected fluxes, and the emission-line equivalent widths, which, to first order, are insensitive to the effects of dust (Kobulnicky & Phillips 2003). In the presence of all these systematic effects, we want to determine whether we can measure the "integrated" gas-phase abundance of a disk galaxy, and, if so, how we can physically interpret that measurement.

Previous efforts investigating the integrated abundances of spiral galaxies found that integrated spectroscopy provides a fairly reliable measure of the gas-phase abundance (Kobulnicky et al. 1999; Pilyugin et al. 2004a). However, these studies synthesized integrated spectra by co-adding observations of individual H II regions; therefore, they could not investigate the systematic effects of DIG emission and dust reddening. Recently, we have obtained spatially unbiased (integrated) spectroscopy for several hundred nearby galaxies (Moustakas & Kennicutt 2006, hereafter MK06). Here, we combine these data with spectroscopy of individual H II regions culled from the literature to investigate whether chemical analysis methods can be used to estimate the metallicities of spatially unresolved star-forming galaxies.

2. DATA

2.1. *Sample Selection and Emission-Line Measurements*

Investigating the integrated nebular abundances of disk galaxies quantitatively poses several observational challenges. First, because of practical considerations, H II-region abundance measurements are generally only available for nearby galaxies subtending relatively large ($\gtrsim 2'$) angular diameters on the sky. At the same time, obtaining an integrated spectrum of an object that is larger than the typical length of a long-slit ($3'-5'$) can be very difficult. Nevertheless, our survey (MK06) includes among the first integrated spectra of spiral galaxies with measurable radial abundance gradients.

As part of a larger effort to study extra-galactic star formation, we have obtained integrated, optical ($3600-6900$ Å) spectrophotometry at ~ 8 Å FWHM resolution for a diverse sample of 417 nearby (< 150 Mpc) galaxies (MK06). Our survey implements the Kennicutt (1992) long-slit drift-scanning technique to obtain integrated spectra of large galaxies at the spectral resolution afforded by a $2\farcs5 \times 200''$ long-slit (see also Jansen et al. 2000; Gavazzi et al. 2004). The size of each galaxy at the B_{25} mag arcsec^{-2} isophote dictates the parameters of the drift-scan, and the width of the extraction aperture. The resulting spectra typically include $80-100\%$ of the optical light. These observations are ideally suited to our analysis because they are analogous to obtaining a normal (spatially fixed) optical spectrum of a distant galaxy, which subtends a corresponding smaller angular diameter on the sky.

In MK06 we present the fluxes and equivalent widths (EWs) of the strong nebular emission lines, including [O II] λ3727, [O III] λ5007, [N II] λ6584, Hα, and Hβ, for the complete sample of galaxies. Hereafter, we assume that [O III] λ4959 is 0.34 times the [O III] λ5007 intensity, as determined by atomic physics (Storey & Zeippen 2000). Unfortunately, the temperature-sensitive [O III] λ4363 line is typically not detected in our spectra, which is not surprising given that this line becomes vanishingly weak in metal-rich galaxies (e.g., Kennicutt et al. 2003); therefore, we must rely on so-called strong-line calibrations to estimate the oxygen abundance (see §3.1).

The nebular line measurements presented in MK06 include a careful treatment of underlying stellar absorption, which is among the most important systematic effects to consider in any emission-line abundance analysis. In spectroscopic studies of individual H II regions, the Balmer lines are typically corrected for a constant ~ 2 Å of stellar absorption, corresponding to the amount of absorption expected for a young ($\lesssim 20$ Myr) stellar population (e.g., McCall et al. 1985; Olofsson 1995). However, in general, the integrated, luminosity-weighted stellar population of a galaxy will differ considerably from that of a single star-forming region. In particular, the assumption of a constant amount of stellar absorption for Hα and Hβ may break down, since different stellar populations will dominate the integrated light at red (~ 6500 Å) and blue (~ 4800 Å) wavelengths, according to the particular star-formation history of each galaxy. Moreover, the exact correction depends on spectral resolution, since the nebular lines are typically narrower than the underlying absorption.

To address these issues, in MK06 we use population synthesis to model the integrated absorption-line spectrum of each galaxy in our sample. We fit a non-negative linear combination of seven instantaneous-burst Bruzual & Charlot (2003) population synthesis models, convolved to the instrumental resolution, with ages ranging from 5 Myr to 12 Gyr. Including a simple treatment of dust reddening, this method results in precise subtraction of the stellar continuum underlying the nebular emission lines (see also Ho et al. 1997; Tremonti et al. 2004; Cid Fernandes et al. 2005). For the subset of galaxies considered in this analysis (see below), the Hβ absorption ranges from 2.8 to 4.9 Å, with a mean value of 3.9 ± 0.5 Å. The corresponding correction for Hα is $1.8-3.0$ Å, with a mean of 2.5 ± 0.3 Å.

We define our sample according to two selection criteria. First, we restrict the objects observed by MK06 to spiral galaxies with well-detected (3σ) Hα and Hβ emission lines. We also reject galaxies whose integrated emission-line spectrum is clearly dominated by an active nucleus (e.g., NGC 1068). Next, we conduct a search of the literature for spectroscopy of individual H II regions in the remaining objects.[3] Our search results in data on 252 H II regions in 14 disk galaxies. The median number of H II regions per galaxy is 15. One ob-

[3] We only consider observations that include the [O II], [O III], and Hβ nebular lines, since these are the most likely lines to be measured in distant galaxies. This requirement eliminates the imaging spectrophotometric data of the galaxies in our sample presented by Dutil & Roy (1999), Martin & Roy (1992), and Martin & Belley (1997), among others.

ject, NGC 4713, has fewer than six H II regions, which Zaritsky et al. (1994) advocate as the minimum number of regions needed to robustly determine the abundance gradient (see also Dutil & Roy 2001). Nevertheless, we retain NGC 4713 in our sample, bearing in mind that the derived abundance gradient may be subject to additional systematic uncertainty. To place the size of our sample in context, these 14 objects account for $\sim 1/4$ of the total number of galaxies with measurable abundance gradients (e.g., Pilyugin et al. 2004b).

In Table 1 we list the galaxies in our sample and the global properties relevant to our analysis. Column (2) gives the morphological type of each object from de Vaucouleurs et al. (1991, hereafter RC3). Column (3) lists the absolute B-band magnitude, based on the Galactic extinction-corrected B-band magnitude ($R_V = 3.1$; Schlegel et al. 1998; O'Donnell 1994) and distance tabulated in MK06. Column (4) lists ρ_{25}, the radius of the semi-major axis at the B_{25} mag arcsec^{-2} isophote from the RC3. In columns (5) and (6), respectively, we list the photometric inclination angle and position angle, as determined in the K_s-band (Jarrett et al. 2000, 2003). To compute the inclination angle we use the observed major-to-minor axis ratio at the $K_{s,20}$ mag arcsec^{-2} isophote (Jarrett et al. 2000, 2003), and assume that the axial ratio of a system viewed edge-on is 0.2 (Tully et al. 1998). For NGC 5194, however, we use the kinematic inclination angle determined by Tully (1974). Finally, in column (7) we give the Hα surface brightness, $\Sigma(\mathrm{H}\alpha) = 4.5 \times 10^{44} I(\mathrm{H}\alpha)/\rho_{25}^2$ in erg s^{-1} pc^{-2}, where $I(\mathrm{H}\alpha)$ is the Hα flux in erg s^{-1} cm^{-2} from MK06, corrected for extinction as described in §3.1. The remaining columns in Table 1 are described in §3.1.

For each H II region drawn from the literature, we tabulate the coordinates relative to the galactic nucleus, and the stellar absorption and reddening-corrected [O II] λ3727, [O III] λ5007, and Hβ emission-line flux measurements and uncertainties. As before, we set [O III] λ4959 = 0.34 × [O III] λ5007. Using the optical disk radius and galactic position and inclination angles given in Table 1, we also compute the de-projected galactocentric radius of each H II region, normalized to ρ_{25}. In §3.2 we use these data to determine the radial abundance gradients for the galaxies in our sample.

2.2. *Sample Properties and Selection Biases*

In this section we discuss some of the sample selection biases. As alluded to in §2.1, the size of the sample is determined by simultaneously requiring integrated spectroscopy *and* spectroscopy for a sufficient number of individual H II regions. In terms of B-band luminosity, the sample is generally biased toward bright galaxies, since lower-luminosity galaxies tend not to exhibit abundance gradients. We note, however, that our sample spans more than an order-of-magnitude in B-band luminosity, from $M_B = -18.2$ to -21.0 mag. For comparison, the absolute B magnitudes of the disk galaxies studied by Pilyugin et al. (2004b), which is the most comprehensive compilation of galaxies with measured abundance gradients to date, range from -17.8 to -21.6 mag. The distribution of inclination angles in our sample is fairly broad, ranging from 11° in NGC 3344, to 72° in NGC 3198; the mean inclination angle is $41° \pm 19°$. In §4 we test whether variations in inclination along the line-of-sight systematically biases the integrated abundances.

The distribution of morphological types in our sample is weighted toward late-type galaxies: 85% of the sample is type Sbc or later, with only two early-type objects, NGC 3351 (Sb) and NGC 4736 (Sab). This bias arises because of observational and physical selection effects which tend to prefer late-type galaxies. For example, the number of early-type galaxies with measured abundance gradients is relatively limited, because H II regions in early-type galaxies are rarer and have lower luminosities and surface brightnesses than corresponding H II regions in late-type galaxies (e.g., Kennicutt 1988). Previous studies have found that early-type galaxies are, on average, more metal rich, and have shallower abundance gradients than late-type galaxies (e.g., Garnett & Shields 1987; Oey & Kennicutt 1993; Zaritsky et al. 1994; Dutil & Roy 1999). We note, however, that our sample includes galaxies that are as luminous and metal-rich as other well-known early-type disk galaxies such as M 81 (Garnett & Shields 1987). A related selection effect is that in the integrated spectra of early-type galaxies the equivalent widths of the nebular lines, if present, tend to be significantly lower than the corresponding emission-line equivalent widths in late-type galaxies. This observation can be attributed to the lower star-formation rate per unit luminosity or mass in early-type galaxies (e.g., Caldwell et al. 1991; Kennicutt et al. 1994).

Despite the relatively small number of early-type galaxies, we argue that our sample is still representative for the kind of analysis we are conducting, and that our conclusions are not strongly affected by this morphological bias. In particular, the objects most likely to be studied at high redshift should have higher gas resevoirs, high specific star-formation rates, and large emission-line equivalent widths. For example, in an analysis of 64 star-forming galaxies at $0.3 < z < 0.8$, Kobulnicky et al. (2003) found an average Hβ emission-line EW of 21 ± 14 Å, while Pettini et al. (2001) measured Hβ EWs in excess of ~ 20 Å in a sample of five Lyman-break galaxies at $z \sim 3$. Finally, since early-type galaxies tend to have shallow abundance gradients, small amounts of dust, and a weak or absent DIG phase, we do not expect the integrated abundances of early-type galaxies to differ significantly from the abundances infered from spectroscopy of individual H II regions.

3. ANALYSIS

3.1. *Integrated Abundances*

We use the emission-line measurements from MK06 to compute the integrated oxygen abundances of the galaxies selected in §2.1. A principal assumption of this method is that the observed emission lines arise via photoionization from massive stars. Consequently, it is important to assess any possible contamination from nuclear activity in our integrated emission-line spectra. Ho et al. (1997) have obtained nuclear spectra of all the galaxies in our sample; they find that 50% (7/14) have H II-like nuclei, 36% (5/14) are LINERs or transition objects, and 14% (2/14) exhibit Seyfert 2 nuclear line-ratios. In all cases, however, we find that the nucleus contributes < 3% to the integrated Hα flux. Therefore, we can apply standard techniques to derive chemical abun-

dances from the observed emission-line spectra.

From the observed Hα/Hβ ratio, we estimate the nebular reddening assuming an intrinsic ratio of 2.86 and the O'Donnell (1994) Milky Way extinction curve (listed in col. [8] of Table 1). The distribution of reddening values for the sample ranges from 0.08 to 0.69 mag, with a mean value of 0.31 ± 0.17 mag. Moustakas et al. (2006) show that adopting a simple Milky Way extinction law works remarkably well at accounting for the effects of dust on the nebular lines from integrated optical spectra (see also Kewley et al. 2002), despite the wide variation in attenuation laws predicted by theoretical models (e.g., Witt & Gordon 2000; Fischera & Dopita 2005).

To investigate the systematic effect of dust attenuation, we inter-compare the abundances determined using the observed (un-corrected) emission-line fluxes, the reddening-corrected fluxes, and the emission-line EWs. Kobulnicky & Phillips (2003) have suggested replacing fluxes with EWs when determining the integrated emission-line abundances of galaxies, since, to first order, EWs are insensitive to dust attenuation. However, the EW method for deriving abundances is sensitive to intrinsic variations in the stellar populations, and to differential extinction between the lines and the continuum, as we discuss in §4.

We explore the effect of choosing a particular strong-line calibration by computing abundances using both the McGaugh (1991, hereafter M91) and the Pilyugin & Thuan (2005, hereafter PT05) calibrations of the $R_{23} \equiv ([\mathrm{O\ II}]\ \lambda 3727 + [\mathrm{O\ III}]\ \lambda\lambda 4959, 5007)/\mathrm{H}\beta$ parameter. We focus on the R_{23} parameter as an abundance diagnostic because the oxygen and Hβ lines are among the strongest optical emission lines, and they are observable in ground-based optical spectra to $z \sim 1$. Both calibrations account for variations in ionization parameter at fixed metallicity, either through the [O III]/[O II] ratio (M91), or the [O III]/([O II]+[O III]) ratio (PT05). The M91 calibration, as parameterized by Kobulnicky et al. (1999), is based on an extensive grid of photoionization models spanning a wide range of metallicity and ionization parameter. By comparison, PT05 have constructed a purely empirical calibration, based on a carefully selected sample of H II regions with well-measured electron temperatures. Finally, we note that although R_{23} is double-valued as a function of abundance (see, e.g., M91), all the galaxies in our sample lie on the upper branch of the relation between R_{23} and (O/H).

On average, the M91 abundance scale is shifted to higher values relative to the PT05 scale by ~ 0.5 dex, or a factor of ~ 3 (see Fig. 2). In §4 we show that selecting among the M91 and PT05 calibrations has a significant effect on the absolute oxygen abundances, and a modest effect on the slope of the derived abundance gradients, but does not significantly alter our conclusions. Using a different theoretical calibration in place of M91 (e.g., Zaritsky et al. 1994; Kewley & Dopita 2002; Kobulnicky & Kewley 2004) has a negligible effect on our conclusions.

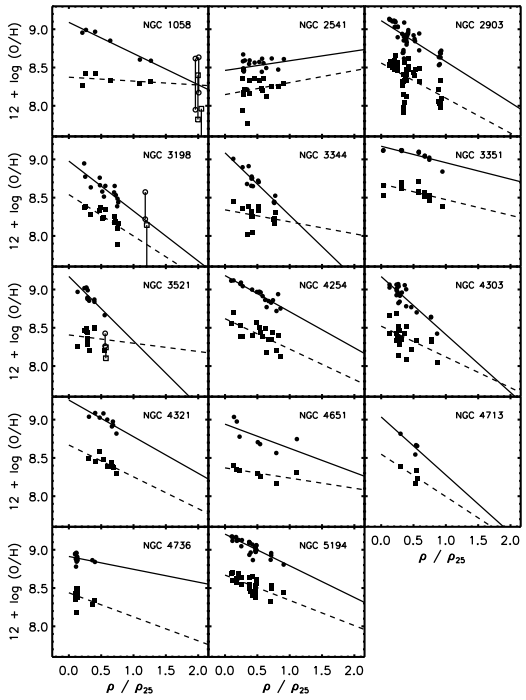

FIG. 1.— Oxygen abundance vs. de-projected galactocentric radius, ρ, normalized to ρ_{25}, the disk radius at the B_{25} mag arcsec^{-2} isophote. Oxygen abundances for each H II region have been computed using both the McGaugh (1991, M91) (*circles*) and the Pilyugin & Thuan (2005, PT05) (*squares*) abundance calibrations. The solid line is the best fit through the M91 abundance distribution, and the dashed line is the corresponding fit through the PT05 abundances. H II regions that have been excluded from the fits are shown as open symbols, with a vertical line connecting the upper- and lower-branch abundances (see §3.2 for details).

In Columns (9)–(11) of Table 1 we list the three integrated abundances and statistical uncertainties derived using the M91 abundance calibration; columns (12)–(14) give the corresponding abundances based on the PT05 calibration. In every object except NGC 3351 and NGC 4321, the two dustiest galaxies in the sample, we detect the [O II], [O III], and Hβ emission lines with $> 3\sigma$ significance. In NGC 3351 and NGC 4321, however, we derive an upper limit to the [O II] flux and EW, which translates into a lower limit on the oxygen abundance.

3.2. *H II-Region Abundance Gradients*

We compute the radial abundance gradient of each galaxy in our sample using an unweighted linear least-squares fit to both the M91 and the PT05 H II-region abundances. To quantify the uncertainty in the gradient, we re-compute the fit 500 times, modulating the metallicity of each H II region by a Gaussian distribution with a width equal to the statistical uncertainty. Table 2 and Figure 1 present the results of our fits. Columns (2)–(4) of Table 2 are based on the M91 abundance calibration and list, respectively, the extrapolated central abundance at galactocentric radius $\rho = 0$, the *characteristic* abundance, defined as the oxygen abundance at $\rho = 0.4\,\rho_{25}$ (Zaritsky et al. 1994; Garnett 2002), and the slope of the abundance gradient in dex ρ_{25}^{-1}. Columns (5)–(7) give the corresponding quantities derived using the PT05 abundance calibration. Finally, columns (8) and (9) give the number of H II regions used in the fit,

and the corresponding references to the literature, respectively.

In Figure 1 we plot the normalized galactocentric radius, ρ/ρ_{25}, versus oxygen abundance for the H II regions in each galaxy. The circles and squares distinguish the M91 and PT05 abundances, respectively. We assume that all the H II regions lie on the upper branch of the appropriate R_{23}-(O/H) relation, except as noted below. The solid line is the best fit through the M91 abundance distribution, and the dashed line is the corresponding fit through the PT05 H II-region abundances.

We exclude a handful of H II regions from the fits, shown in Figure 1 as open symbols without error bars, with a solid vertical line connecting the upper- and lower-branch R_{23} abundances. Specifically, in NGC 1058 we exclude the two outermost H II regions, FGW1058G and FGW1058H (Ferguson et al. 1998), because they are well outside the main optical disk of the galaxy. We also exclude the outermost H II region in NGC 3198, –027–187 (Zaritsky et al. 1994), which has an extremely low ionization parameter, $\log([\mathrm{O\ III}]/[\mathrm{O\ II}]) = -0.76$. Unfortunately, the strong-line calibrations used here fail at reproducing the ionization properties of this object, which leads to the unphysical situation of having a lower-branch abundance that is several times higher than the corresponding upper-branch abundance. Finally, we also reject the anomolously low-metallicity H II region in NGC 3521, –033–118 (Zaritsky et al. 1994), which has a negligible effect on the derived abundance gradient.

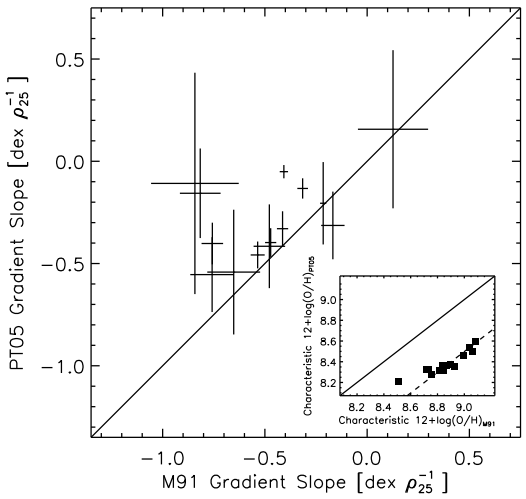

FIG. 2.— Slope of the radial abundance gradient determined from fitting to the Pilyugin & Thuan (2005, PT05) abundance distribution vs. the corresponding slope derived from fitting to the McGaugh (1991, M91) H II-region abundances (see Fig. 1). (*Inset*) Correlation between the *characteristic* oxygen abundances (see §3.2 and Table 2 for details). The dashed line shows the 0.5 dex mean offset between the M91 and PT05 abundance scales, while the solid line in both panels is the line-of-equality.

In Figure 2 we compare the slope of the gradients derived using the M91 and PT05 abundance calibrations, and a comparison of the characteristic abundances (*inset*). The solid line in both panels is the line-of-equality, and the dashed line in the inset shows the median 0.5 dex offset between the M91 and PT05 abundances. The two slopes generally correlate, although the PT05 gradients are systematically shallower than the corresponding gradients derived using the M91 oxygen abundances. The four most discrepant examples are NGC 3521, NGC 3344, NGC 1058, and NGC 4303. In all cases, the PT05 calibration predicts a much flatter relationship between galactocentric position and oxygen abundance, a result which has profound implications for our understanding of the chemical evolution properties of spiral galaxies (e.g., Molla et al. 1996; Pilyugin et al. 2006). Exploring this result in more detail, however, is beyond the scope of this paper.

4. RESULTS

Figures 3 and 4 illustrate the principal result of this paper. Here we plot the characteristic oxygen abundance, as derived from the H II-region abundance gradient (Fig. 1, Table 2), versus our three estimates of the integrated abundance. We plot the integrated "observed", "reddening-corrected", and "EW" abundances using open circles, filled circles, and open squares, respectively, and the lower limits to the integrated abundances in NGC 3351 and NGC 4321 as arrows (§3.1 and Table 1).

As an independent check on our results, in Figure 3 we show the integrated abundances determined by Kobulnicky et al. (1999), against the characteristic H II-region abundances from Zaritsky et al. (1994) (*filled grey triangles*). Kobulnicky et al. (1999) derive pseudo-integrated abundances for their sample of 22 galaxies, nine of which are common to our sample, by dividing each object into $5-13$ equal-size radial zones and convolving the observed Hα surface-brightness distribution with the reddening-corrected H II-region line-strengths from Zaritsky et al. (1994). We subtract 0.2 dex from these points to place them on the M91 abundance scale.

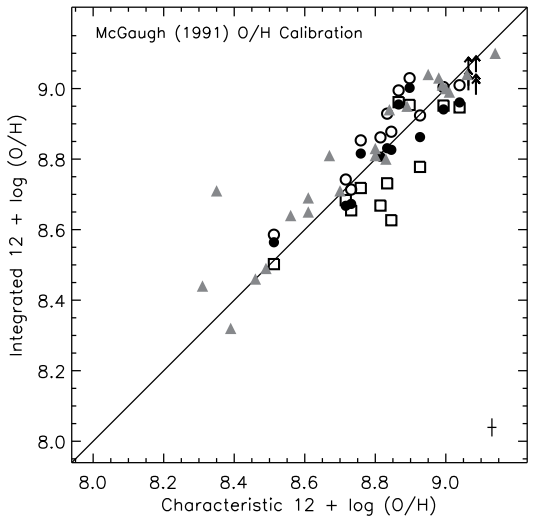

FIG. 3.— Characteristic vs. integrated oxygen abundance, based on the McGaugh (1991) abundance calibration. Symbols differentiate between abundances computed using the observed emission-line fluxes (*open circles*), the reddening-corrected fluxes (*filled circles*), and the emission-line equivalent widths (*open squares*). For comparison we plot the results from Kobulnicky et al. (1999) using filled grey triangles, accounting for the 0.2 dex offset between the Zaritsky et al. (1994) and McGaugh (1991) abundance scales. Lower limits to the oxygen abundance in NGC 3351 and NGC 4321 are shown as arrows. The cross shows the median measurement uncertainty of the data.

Examining Figures 3 and 4, we find that all three integrated abundances correlate with the characteristic, or

spatially resolved abundance, independent of the abundance calibration used. A Spearman rank correlation test quantifies the significance of the observed correlations at $> 99\%$. We conclude, therefore, that, to first order, the abundance inferred from the integrated emission-line spectrum of a galaxy is representative of the gas-phase oxygen abundance at $\rho = 0.4\,\rho_{25}$, even in the presence of an abundance gradient, contributions from DIG emission, and variations in dust reddening.

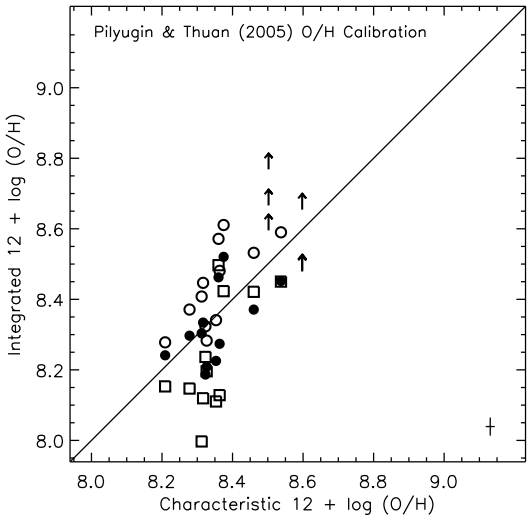

FIG. 4.— Same as Fig. 3, but using the Pilyugin & Thuan (2005) abundance calibration.

Table 3 presents the mean, standard deviation, and median of the residuals we measure between the integrated and characteristic abundances. On average, the integrated abundance inferred from the observed (un-corrected) line-fluxes overestimates the characteristic abundance by 0.05 ± 0.06 dex or 0.09 ± 0.08 dex using the M91 or PT05 calibration, respectively. Accounting for dust reddening using a simple Milky Way extinction curve (O'Donnell 1994) removes the systematic offset, but has almost no effect on the residual scatter. This result is consistent with other recent studies, which find that the integrated emission lines of nearby star-forming galaxies appear to be attenuated by a simple foreground dust screen, and that the integrated Balmer decrement is a robust indicator of the amount of dust (e.g., Calzetti et al. 1994; Jansen et al. 2001; Kewley et al. 2002; Dopita et al. 2002; Moustakas et al. 2006). The relatively small wavelength separation between [O II] λ3727 and Hβ λ4861, and the broad similarity of extinction and attenuation curves in the optical, additionally help to minimize the effects of dust.

The integrated abundances determined from the emission-line EWs, by comparison, systematically *underestimate* the characteristic abundance. The mean offset is -0.06 ± 0.09 dex using the M91 calibration, or -0.11 ± 0.13 dex using the PT05 calibration. The median offsets are slightly smaller, -0.04 dex and -0.09 dex, respectively. Kobulnicky & Phillips (2003) discuss in detail the systematic effects of using EWs to determine integrated abundances. In particular, following their recommendation, we have assumed that $\alpha = 1$, where α is related to the ratio of the intrinsic continuum between 3727 Å and 4861 Å, and the differential extinction between the stellar continuum and the emission lines (see Kobulnicky & Phillips 2003, their eq. [7]). Assuming $\alpha = 0.9$, which is well within the expected range of this parameter ($\alpha = 0.84 \pm 0.3$; Kobulnicky & Phillips 2003), increases the M91 integrated EW abundances by a median $+0.04$ dex, and the corresponding PT05 abundances by $+0.06$ dex. We conclude, therefore, that the integrated EW abundances are consistent with the characteristic gas-phase abundances, provided that an appropriate choice for α is made for the sample under consideration. We attribute the increased scatter in the integrated EW abundances relative to the abundances based on the line-fluxes to variations in α among star-forming galaxies. We note, however, that the measured scatter is comparable to the ± 0.1 dex precision of the EW abundance technique (Kobulnicky & Phillips 2003).

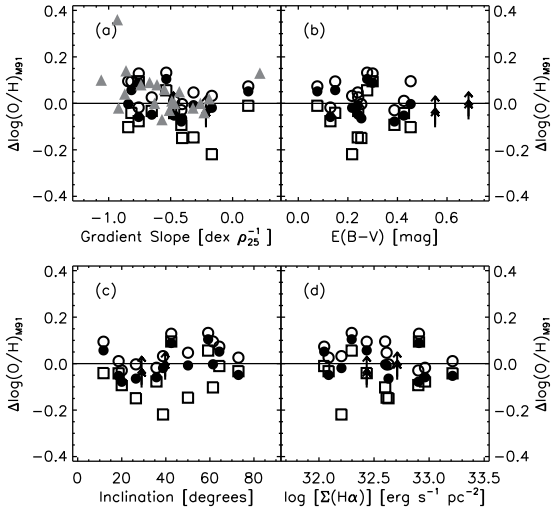

FIG. 5.— Oxygen abundance residuals (integrated minus characteristic abundance) based on the McGaugh (1991) calibration vs. (*a*) the slope of the abundance gradient, (*b*) dust reddening, (*c*) inclination angle, and (*d*) Hα surface brightness. Symbols are as in Fig. 3.

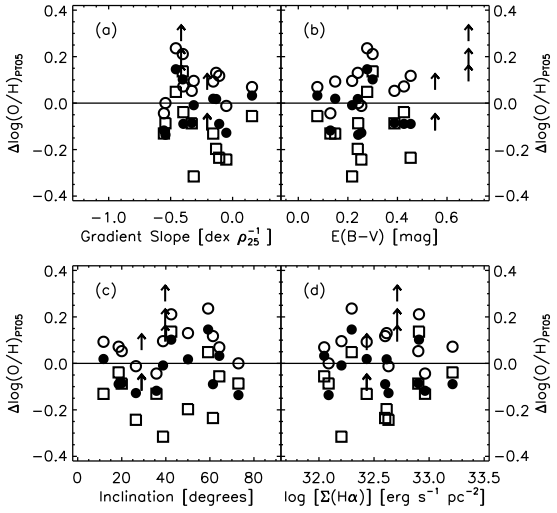

FIG. 6.— Same as Fig. 5, but using the Pilyugin & Thuan (2005) abundance calibration.

Next, we investigate the physical origin of the residual scatter between the integrated and characteristic abundances. In Figure 5 we plot the abundance residuals based on the M91 calibration, versus various physical properties of the sample: (*a*) the slope of the abundance gradient, (*b*) dust reddening, (*c*) inclination angle, and (*d*) Hα surface brightness, Σ(Hα), which characterizes the disk star-formation rate (SFR) per unit area (Kennicutt 1998). For our sample Σ(Hα) spans a factor of ~ 15, comparable to the range in $\Sigma(\mathrm{H}\alpha) \propto \Sigma(\mathrm{SFR})$ found by Kennicutt (1998) for a larger sample of normal disk galaxies. The corresponding residual plots using the PT05 abundance calibration are shown in Figure 6. Table 4 presents the Spearman rank correlation coefficients for each residual plot, and the probability that the variables are *uncorrelated*.

Examining Figures 5–6 and Table 4, we find that the residuals are not highly correlated with *any* of the variables we have considered. We find a marginally significant ($\geq 80\%$ probability) correlation between the observed and reddening-corrected M91 abundance residuals, and the galaxy inclination angle (Fig. 5*c*). We also find a marginally significant anti-correlation between these residuals and Σ(Hα) (Fig. 5*d*). None of the residual correlations using the PT05 calibration are significant, although the increased scatter in the PT05 abundances (Fig. 1, Table 3) may be masking any underlying trends.

The positive correlation between the abundance residuals and inclination angle, if it exists, is opposite of what we would have expected. The correlation indicates that the integrated abundance of an edge-on galaxy is *higher* than the corresponding metallicity of a less-inclined galaxy. Given the existence of radial abundance gradients (e.g., Fig. 1), we would have anticipated the integrated spectrum of an inclined galaxy to be weighted more toward the outer, metal-poor H II regions. This exact trend is shown by Tremonti et al. (2004, their Fig. 7) as a strong correlation between the residuals of the stellar-mass metallicity relation and inclination angle, based on an analysis of $\sim 50,000$ star-forming galaxies in the Sloan Digital Sky Survey. Tremonti et al. (2004) find that edge-on galaxies may appear, on average, 0.2 dex (60%) more metal-rich than face-on galaxies. Since this systematic difference is comparable to the amount of chemical enrichment between the present day and $z \sim 1$ (e.g., J. Moustakas et al. 2006, in preparation; Kobulnicky et al. 2003; Kobulnicky & Kewley 2004), sample selection effects that may be biased with respect to inclination angle should be carefully considered in look-back studies of galactic chemical evolution (e.g., Tully-Fisher studies; Mouhcine et al. 2006).

Since the strength of low-ionization line-ratios such as [N II]/Hα and [S II]/Hα correlate with the Hα surface brightness (e.g., Wang et al. 1998), indicating a prominent DIG phase, the lack of a significant correlation between Σ(Hα) and the abundance residuals in Figures 5*d* and 6*d* suggests that integrated abundance measurements are relatively unaffected by DIG emission. To explore this result in more detail, in Figure 7 we plot two emission-line diagnostic diagrams for our sample (*squares*), all the star-forming galaxies with integrated spectroscopy in the MK06 survey (*diamonds*), individual H II regions drawn from a diverse sample of disk and dwarf galaxies (*grey points*; McCall et al. 1985; Zaritsky et al. 1994; van Zee et al. 1998; Izotov & Thuan 1998), and regions of DIG in three disk galaxies (*crosses*), NGC 0598=M 33, NGC 5194=M 51a, and NGC 0223=M 31, based on deep long-slit spectroscopy by Galarza et al. (1999) and Hoopes & Walterbos (2003).

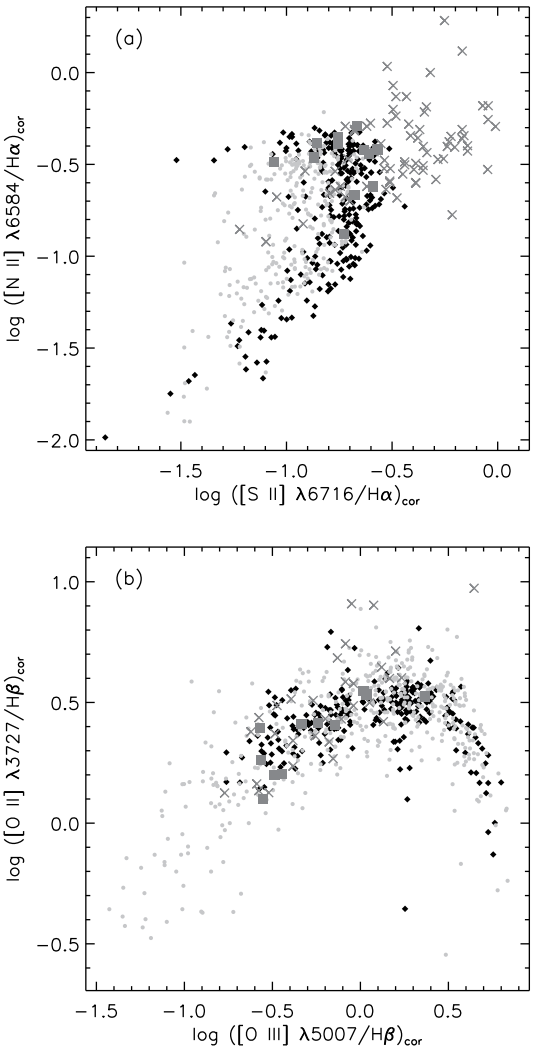

FIG. 7.— Diagnostic diagrams showing the emission-line sequences traced by our sample (*squares*), the full sample of star-forming galaxies from Moustakas & Kennicutt (2006) (*diamonds*), H II regions (*grey points*), and regions of diffuse-ionized gas in M 33, M 51a, and M 31 (*crosses*), as described in §4. (*a*) Reddening-corrected [S II] λ6716/Hα ratio vs. [N II] λ6584/Hα. (*b*) Reddening-corrected [O III] λ5007/Hβ ratio vs. [O II] λ3727/Hβ.

Figure 7*a* shows that H II regions and galaxies trace out similar emission-line sequences in the [N II]/Hα versus [S II]/Hα plane (corrected for reddening), while the DIG regions extend to much higher values of both [N II]/Hα and [S II]/Hα. Moreover, we observe that the integrated line-ratios preferentially lie at or above the upper envelope defined by the H II regions (see also Lehnert & Heckman 1994). The enhancement of low-ionization lines in the DIG is generally attributed to a low ionization parameter (e.g., Domgorgen & Mathis 1994;

Martin 1997). Alternatively, recent self-consistent theoretical models of aging star-forming regions reveal that old, low surface-brightness H II regions exhibit higher [N II]/Hα and [S II]/Hα ratios relative to young, luminous H II regions (M. Dopita 2006, private communication). Regardless of its physical origin, our integrated spectra show a clear enhancement of low-ionization emission relative to H II regions. One implication of this result is that [N II]- or [S II]-based strong-line abundance diagnostics applied to integrated spectra of galaxies (e.g., Charlot & Longhetti 2001; Denicoló et al. 2002; Pettini & Pagel 2004) may be moderately biased toward higher metallicities.

In Figure 7*b* we plot the reddening-corrected [O III]/Hβ ratio versus [O II]/Hβ. In this diagram the emission-line sequences defined by galaxies, H II regions, and regions of DIG generally overlap. Unlike [N II]/Hα and [S II]/Hα, lines of constant ionization parameter run nearly parallel to the [O III]/Hβ versus [O II]/Hβ emission-line sequence (e.g., Kewley & Dopita 2002). We conclude, therefore, that measurements based on the globally averaged R_{23} parameter give abundances that are fairly representative of the gas-phase oxygen abundances of galaxies.

We conclude this section by testing one of the principal assumptions of the preceding analysis. Following Zaritsky et al. (1994), we have defined the characteristic abundance of a disk galaxy as the oxygen abundance at $\rho = 0.4\,\rho_{25}$ (see also Garnett et al. 1997; Garnett 2002). However, given the form of the abundance gradient, we can *derive* the normalized galactocentric radius, $\rho_{\rm int}/\rho_{25}$, where the integrated abundance equals the gas-phase abundance, assuming that the reddening-corrected integrated abundance is a perfect measure of the gas-phase abundance. For this calculation we only consider the M91 abundance calibration, which produces smaller uncertainties in the gradient slopes; we also exclude NGC 2541, which exhibits an increasing abundance with radius (although the slope is formally consistent with zero).

We find that $\rho_{\rm int}/\rho_{25}$ ranges from 0.2 in NGC 2903, to 0.8 in NGC 3344, with a mean value of 0.47 ± 0.15. Not surprisingly, $\rho_{\rm int}/\rho_{25}$ correlates with the slope of the abundance gradient, in the sense that the integrated abundances of galaxies with steeper abundance gradients are systematically higher than the integrated abundances of galaxies with shallower gradients. We conclude, therefore, that the dominant source of scatter in the abundance residuals found in Figures 5–6 (see also Table 3) is due to assuming a fixed $\rho_{int}/\rho_{25} = 0.4$. Our analysis shows that while this is a reasonable average assumption, the exact radius does vary from object-to-object in a way that depends mildly on the slope of the abundance gradient.

5. DISCUSSION & SUMMARY

In this paper we have investigated whether spatially unresolved (integrated) spectroscopy of a spiral galaxy can be used to infer its mean interstellar oxygen abundance, as measured from observations of individual H II regions. Our analysis makes use of a new integrated spectrophotometric survey of nearby star-forming galaxies presented by Moustakas & Kennicutt (2006), and observations of more than 250 H II regions culled from the literature. Our final sample consists of 14, predominantly late-type spiral galaxies spanning a wide range of B-band luminosity, inclination angle, Hα surface brightness, and dust content (Table 1). For the first time, these data allow us to investigate the systematic effects of diffuse-ionized gas emission, dust reddening, and the slope of the abundance gradient on the determination of integrated abundances.

We derive integrated oxygen abundances using the emission-line measurements presented by Moustakas & Kennicutt (2006), who carry out a careful treatment of underlying stellar absorption. We apply both a theoretical (McGaugh 1991), and an empirical (Pilyugin & Thuan 2005) strong-line (R_{23}) abundance calibration to the observed emission-line fluxes, the reddening-corrected fluxes, and the emission-line equivalent widths (following Kobulnicky & Phillips 2003). We analyze the H II-region data compiled from the literature self-consistently; in particular, we determine the H II-region abundances using the same abundance calibration applied to the integrated emission lines, and we compute the de-projected galactocentric position of each object using robust inclination and position angles determined in the near-infrared. With these measurements, we derive the form of the abundance gradient for each galaxy in our sample (Fig. 1, Table 2).

Our principal result is that the integrated abundance of a normal disk galaxy correlates well with its *characteristic* gas-phase abundance, or the H II-region abundance measured at $\rho = 0.4\,\rho_{25}$ (Figs. 3 and 4). The typical scatter in the correlation is ± 0.1 dex, independent of whether the McGaugh (1991) or the Pilyugin & Thuan (2005) calibration is used (Table 3). We note, however, that the scatter in the abundance residuals is generally higher when using the Pilyugin & Thuan calibration. These results confirm and extend the analysis carried out by Kobulnicky et al. (1999) and Pilyugin et al. (2004a), who used simulated integrated galaxy spectra. Integrated abundances based on the observed emission-line fluxes, or the emission-line equivalent widths (Kobulnicky & Phillips 2003) are susceptible to additional systematic effects of order $0.05 - 0.1$ dex with respect to the abundances based on the reddening-corrected fluxes, at least for the range of reddenings and stellar populations spanned by our sample. The systematic residuals using the equivalent-width method, however, can be minimized or eliminated by adopting a different value of α (see §4 and Kobulnicky & Phillips 2003).

We studied the residuals between the integrated and characteristic abundances of the galaxies in our sample to identify a physical origin for the source of the scatter. We found no significant correlations between the residuals and the slope of the abundance gradient, the dust reddening, the inclination angle, or the Hα surface brightness (Figs. 5 and 6, and Table 4). We note, however, that Tremonti et al. (2004) found that inclination can significantly bias integrated abundances, in the sense that edge-on galaxies may appear, on average, 0.2 dex more metal-poor than face-on galaxies.

By comparing the emission-line sequences of galaxies, H II regions, and regions of diffuse-ionized gas, we found that the integrated [N II]/Hα and [S II]/Hα ratios of galaxies lie along the upper envelope of the sequence defined by high surface brightness H II regions, consistent

with a modest contribution from diffuse-ionized gas emission to our integrated spectra (Fig. 7). By comparison, the integrated [O III]/Hβ and [O II]/Hβ ratios of galaxies are relatively insensitive to contributions from diffuse-ionized gas emission, suggesting that the R_{23} parameter is a more robust abundance diagnostic for galaxies than strong-line calibrations that rely on either [S II] or [N II].

Finally, we found that the reddening-corrected integrated abundances of the galaxies in our sample were equal to the gas-phase abundance at normalized galactocentric radii ranging from 0.2 to 0.8, depending on the slope of the abundance gradient. On average, the two abundances were equal at $\rho/\rho_{25} = 0.47 \pm 0.15$, indicating that the commonly adopted radius used to define the characteristic abundance of a disk galaxy (i.e., $\rho/\rho_{25} = 0.4$) is a reasonable assumption.

We conclude that the integrated R_{23} parameter of star-forming disk galaxies is a robust tracer of the gas-phase oxygen abundance, even in the presence of a variety of systematic effects. The strength of the Hβ, [O II], and [O III] lines under typical nebular conditions, and their accessibility to ground-based optical spectrographs to $z \sim 1$, ensures that the R_{23} parameter will continue to be used to measure the build-up of heavy elements in the interstellar media of galaxies with cosmic time.

The authors would like to thank Christy Tremonti, Aleks Diamond-Stanic, and Dennis Zaritsky for comments on a draft of the paper that helped improve its content and clarity. We also thank the anonymous referee for several valuable suggestions that led to a much improved version of the paper. Funding for this project has been provided by NSF grant AST-0307386, NASA grant NAG5-8426, and a SINGS grant, provided by NASA through JPL contract 1224769. This research has made use of the NASA/IPAC Extragalactic Database, which is operated by the Jet Propulsion Laboratory, California Institute of Technology, under contract with the National Aeronautics and Space Administration.

REFERENCES

Bresolin, F., Garnett, D. R., & Kennicutt, R. C. 2004, ApJ, 615, 228
Bresolin, F., Kennicutt, R. C., & Garnett, D. R. 1999, ApJ, 510, 104
Bresolin, F., Schaerer, D., González Delgado, R. M., & Stasińska, G. 2005, A&A, 441, 981
Bruzual, G., & Charlot, S. 2003, MNRAS, 344, 1000
Caldwell, N., Kennicutt, R., Phillips, A. C., & Schommer, R. A. 1991, ApJ, 370, 526
Calzetti, D., Harris, J., Gallagher, J. S., Smith, D. A., Conselice, C. J., Homeier, N., & Kewley, L. 2004, AJ, 127, 1405
Calzetti, D., Kinney, A. L., & Storchi-Bergmann, T. 1994, ApJ, 429, 582
Charlot, S. ., & Longhetti, M. 2001, MNRAS, 323, 887
Cid Fernandes, R., Mateus, A., Laerte, S. J., Stasinska, G., & Gomes, J. M. 2005, MNRAS, 358, 363
de Vaucouleurs, G., de Vaucouleurs, A., Corwin, H. G., Buta, R. J., Paturel, G., & Fouque, P. 1991, Third Reference Catalogue of Bright Galaxies (Volume 1-3, XII, 2069 pp. 7 figs.. Springer-Verlag Berlin Heidelberg New York)
Denicoló, G., Terlevich, R., & Terlevich, E. 2002, MNRAS, 330, 69
Diaz, A. I., Terlevich, E., Vilchez, J. M., Pagel, B. E. J., & Edmunds, M. G. 1991, MNRAS, 253, 245
Domgorgen, H., & Mathis, J. S. 1994, ApJ, 428, 647
Dopita, M. A., Pereira, M., Kewley, L. J., & Capaccioli, M. 2002, ApJS, 143, 47
Dutil, Y., & Roy, J. 1999, ApJ, 516, 62
Dutil, Y., & Roy, J.-R. 2001, AJ, 122, 1644
Ferguson, A. M. N., Gallagher, J. S., & Wyse, R. F. G. 1998, AJ, 116, 673
Ferguson, A. M. N., Wyse, R. F. G., Gallagher, J. S., & Hunter, D. A. 1996, AJ, 111, 2265
Fischera, J., & Dopita, M. 2005, ApJ, 619, 340
Galarza, V. C., Walterbos, R. A. M., & Braun, R. 1999, AJ, 118, 2775
Garnett, D. R. 2002, ApJ, 581, 1019
Garnett, D. R., Kennicutt, R. C., & Bresolin, F. 2004, ApJ, 607, L21
Garnett, D. R., & Shields, G. A. 1987, ApJ, 317, 82
Garnett, D. R., Shields, G. A., Skillman, E. D., Sagan, S. P., & Dufour, R. J. 1997, ApJ, 489, 63
Gavazzi, G., Zaccardo, A., Sanvito, G., Boselli, A., & Bonfanti, C. 2004, A&A, 417, 499
Greenawalt, B., Walterbos, R. A. M., Thilker, D., & Hoopes, C. G. 1998, ApJ, 506, 135
Haffner, L. M., Reynolds, R. J., & Tufte, S. L. 1999, ApJ, 523, 223
Henry, R. B. C., Pagel, B. E. J., & Chincarini, G. L. 1994, MNRAS, 266, 421
Henry, R. B. C., Pagel, B. E. J., Lasseter, D. F., & Chincarini, G. L. 1992, MNRAS, 258, 321
Ho, L. C., Filippenko, A. V., & Sargent, W. L. W. 1997, ApJS, 112, 315
Hoopes, C. G., & Walterbos, R. A. M. 2003, ApJ, 586, 902
Izotov, Y. I., & Thuan, T. X. 1998, ApJ, 500, 188
Jansen, R. A., Fabricant, D., Franx, M., & Caldwell, N. 2000, ApJS, 126, 331
Jansen, R. A., Franx, M., & Fabricant, D. 2001, ApJ, 551, 825
Jarrett, T. H., Chester, T., Cutri, R., Schneider, S., Skrutskie, M., & Huchra, J. P. 2000, AJ, 119, 2498
Jarrett, T. H., Chester, T., Cutri, R., Schneider, S. E., & Huchra, J. P. 2003, AJ, 125, 525
Kennicutt, R. C. 1988, ApJ, 334, 144
—. 1992, ApJS, 79, 255
—. 1998, ApJ, 498, 541
Kennicutt, R. C., Bresolin, F., & Garnett, D. R. 2003, ApJ, 591, 801
Kennicutt, R. C., Tamblyn, P., & Congdon, C. E. 1994, ApJ, 435, 22
Kewley, L. J., & Dopita, M. A. 2002, ApJS, 142, 35
Kewley, L. J., Geller, M. J., Jansen, R. A., & Dopita, M. A. 2002, AJ, 124, 3135
Kobulnicky, H. A., Kennicutt, R. C., & Pizagno, J. L. 1999, ApJ, 514, 544
Kobulnicky, H. A., & Kewley, L. J. 2004, ApJ, 617, 240
Kobulnicky, H. A., & Phillips, A. C. 2003, ApJ, 599, 1031
Kobulnicky, H. A., & Skillman, E. D. 1996, ApJ, 471, 211
Kobulnicky, H. A., Willmer, C. N. A., Phillips, A. C., Koo, D. C., Faber, S. M., Weiner, B. J., Sarajedini, V. L., Simard, L., et al. 2003, ApJ, 599, 1006
Lehnert, M. D., & Heckman, T. M. 1994, ApJ, 426, L27
Liang, Y. C., Hammer, F., Flores, H., Elbaz, D., Marcillac, D., & Cesarsky, C. J. 2004, A&A, 423, 867
Lilly, S. J., Carollo, C. M., & Stockton, A. N. 2003, ApJ, 597, 730
Maier, C., Lilly, S. J., Carollo, C. M., Stockton, A., & Brodwin, M. 2005, ApJ, 634, 849
Maier, C., Meisenheimer, K., & Hippelein, H. 2004, A&A, 418, 475
Martin, C. L. 1997, ApJ, 491, 561
Martin, P., & Belley, J. 1997, A&A, 321, 363
Martin, P., & Roy, J.-R. 1992, ApJ, 397, 463
McCall, M. L., Rybski, P. M., & Shields, G. A. 1985, ApJS, 57, 1
McGaugh, S. S. 1991, ApJ, 380, 140
Molla, M., Ferrini, F., & Diaz, A. I. 1996, ApJ, 466, 668
—. 1997, ApJ, 475, 519
Mouhcine, M., Bamford, S. P., Aragón-Salamanca, A., Nakamura, O., & Milvang-Jensen, B. 2006, MNRAS, 517
Moustakas, J., & Kennicutt, R. C. 2006, ApJS, 164, 81
Moustakas, J., Kennicutt, R. C., & Tremonti, C. A. 2006, ApJ, 642, 775
O'Donnell, J. E. 1994, ApJ, 422, 158
Oey, M. S., & Kennicutt, R. C. 1993, ApJ, 411, 137
Olofsson, K. 1995, A&AS, 111, 57

Pettini, M., & Pagel, B. E. J. 2004, MNRAS, 348, L59
Pettini, M., Shapley, A. E., Steidel, C. C., Cuby, J., Dickinson, M., Moorwood, A. F. M., Adelberger, K. L., & Giavalisco, M. 2001, ApJ, 554, 981
Pilyugin, L. S., Contini, T., & Vílchez, J. M. 2004a, A&A, 423, 427
Pilyugin, L. S., & Thuan, T. X. 2005, ApJ, 631, 231
Pilyugin, L. S., Thuan, T. X., & Vílchez, J. M. 2006, MNRAS, 210
Pilyugin, L. S., Vílchez, J. M., & Contini, T. 2004b, A&A, 425, 849
Reynolds, R. J. 1990, in IAU Symp. 139: The Galactic and Extragalactic Background Radiation, ed. S. Bowyer & C. Leinert, 157–169
Savaglio, S., Glazebrook, K., Le Borgne, D., Juneau, S., Abraham, R. G., Chen, H.-W., Crampton, D., McCarthy, P. J., Carlberg, R. G., Marzke, R. O., Roth, K., Jørgensen, I., & Murowinski, R. 2005, ApJ, 635, 260
Schlegel, D. J., Finkbeiner, D. P., & Davis, M. 1998, ApJ, 500, 525
Shields, G. A., Skillman, E. D., & Kennicutt, R. C. 1991, ApJ, 371, 82
Skillman, E. D., Kennicutt, R. C., Shields, G. A., & Zaritsky, D. 1996, ApJ, 462, 147
Storey, P. J., & Zeippen, C. J. 2000, MNRAS, 312, 813
Thilker, D. A., Walterbos, R. A. M., Braun, R., & Hoopes, C. G. 2002, AJ, 124, 3118
Tremonti, C. A., Heckman, T. M., Kauffmann, G., Brinchmann, J., Charlot, S., White, S. D. M., Seibert, M., Peng, E. W., et al. 2004, ApJ, 613, 898
Tully, R. B. 1974, ApJS, 27, 437
Tully, R. B., Pierce, M. J., Huang, J., Saunders, W., Verheijen, M. A. W., & Witchalls, P. L. 1998, AJ, 115, 2264
van Zee, L., Salzer, J. J., Haynes, M. P., O'Donoghue, A. A., & Balonek, T. J. 1998, AJ, 116, 2805
Vila-Costas, M. B., & Edmunds, M. G. 1992, MNRAS, 259, 121
Vilchez, J. M., Edmunds, M. G., & Pagel, B. E. J. 1988, PASP, 100, 1428
Wang, J., Heckman, T. M., & Lehnert, M. D. 1997, ApJ, 491, 114
—. 1998, ApJ, 509, 93
Witt, A. N., & Gordon, K. D. 2000, ApJ, 528, 799
Zaritsky, D., Kennicutt, R. C., & Huchra, J. P. 1994, ApJ, 420, 87
Zurita, A., Rozas, M., & Beckman, J. E. 2000, A&A, 363, 9

TABLE 1
INTEGRATED OXYGEN ABUNDANCES

Galaxy (1)	Type (2)	M_B (mag) (3)	ρ_{25} (arcmin) (4)	i (deg) (5)	θ (deg) (6)	$\log[\Sigma(\mathrm{H}\alpha)]$ (erg s^{-1} pc^{-2}) (7)	$E(B-V)$ (mag) (8)	12+log(O/H)$_{\mathrm{M91}}$[a] Observed (9)	Corrected (10)	EWs (11)	12+log(O/H)$_{\mathrm{PT05}}$[a] Observed (12)	Corrected (13)	EWs (14)
NGC 1058	SA(rs)c	-18.4	1.51	26	95	32.6	0.25 ± 0.08	8.92 ± 0.03	8.86 ± 0.03	8.78 ± 0.05	8.34 ± 0.04	8.23 ± 0.04	8.11 ± 0.06
NGC 2541	SA(s)cd	-18.2	3.15	64	175	32.0	0.08 ± 0.08	8.59 ± 0.04	8.56 ± 0.04	8.50 ± 0.04	8.28 ± 0.04	8.24 ± 0.05	8.15 ± 0.06
NGC 2903	SB(s)d	-20.2	6.30	59	13	32.3	0.28 ± 0.08	9.03 ± 0.02	9.00 ± 0.03	8.95 ± 0.04	8.61 ± 0.05	8.52 ± 0.06	8.42 ± 0.08
NGC 3198	SB(rs)c	-19.9	4.26	72	40	32.1	0.24 ± 0.09	8.74 ± 0.06	8.67 ± 0.07	8.68 ± 0.06	8.32 ± 0.07	8.19 ± 0.09	8.24 ± 0.08
NGC 3344	(R)SAB(r)bc	-19.2	3.54	11	150	32.4	0.15 ± 0.08	8.85 ± 0.03	8.82 ± 0.04	8.72 ± 0.05	8.37 ± 0.05	8.30 ± 0.05	8.15 ± 0.06
NGC 3351	SB(r)b	-19.6	3.71	28	163	32.4	0.55 ± 0.11	> 9.05	> 8.99	> 8.98	> 8.65	> 8.48	> 8.48
NGC 3521	SAB(rs)bc	-20.1	5.48	61	166	32.6	0.45 ± 0.07	8.93 ± 0.02	8.83 ± 0.04	8.73 ± 0.05	8.48 ± 0.03	8.27 ± 0.04	8.13 ± 0.05
NGC 4254	SA(s)c	-20.3	2.69	18	24	33.2	0.43 ± 0.07	9.00 ± 0.01	8.94 ± 0.02	8.95 ± 0.02	8.53 ± 0.02	8.37 ± 0.03	8.42 ± 0.03
NGC 4303	SAB(rs)bc	-20.0	3.23	42	20	32.9	0.30 ± 0.07	8.99 ± 0.01	8.95 ± 0.02	8.96 ± 0.02	8.57 ± 0.02	8.46 ± 0.03	8.50 ± 0.03
NGC 4321	SAB(s)bc	-21.0	3.71	39	108	32.7	0.69 ± 0.09	> 9.04	> 8.99	> 9.01	> 8.77	> 8.60	> 8.67
NGC 4651	SA(rs)c	-20.3	1.99	50	80	32.6	0.24 ± 0.07	8.86 ± 0.02	8.81 ± 0.03	8.67 ± 0.04	8.45 ± 0.03	8.33 ± 0.04	8.12 ± 0.05
NGC 4713	SAB(rs)d	-18.6	1.35	35	50	33.0	0.13 ± 0.07	8.71 ± 0.02	8.67 ± 0.03	8.65 ± 0.03	8.28 ± 0.03	8.21 ± 0.04	8.20 ± 0.04
NGC 4736	(R)SA(r)ab	-19.4	5.61	38	85	32.2	0.22 ± 0.07	8.88 ± 0.02	8.83 ± 0.02	8.63 ± 0.03	8.41 ± 0.02	8.30 ± 0.03	8.00 ± 0.04
NGC 5194	SA(s)bc	-20.7	5.61	20	58	32.9	0.39 ± 0.07	9.01 ± 0.01	8.96 ± 0.02	8.95 ± 0.02	8.59 ± 0.03	8.45 ± 0.03	8.45 ± 0.03

NOTE. — Col. (1) Galaxy name; Col. (2) Morphological type from de Vaucouleurs et al. (1991); Col. (3) Absolute B-band magnitude, corrected for foreground Galactic extinction ($R_V = 3.1$; Schlegel et al. 1998; O'Donnell 1994), based on the apparent magnitude and distance given by Moustakas & Kennicutt (2006); Col. (4) Radius of the major axis at the B_{25} mag arcsec^{-2} isophote from de Vaucouleurs et al. (1991); Col. (5) Galaxy inclination angle based on the K_s-band major-to-minor axis ratio (Jarrett et al. 2000, 2003), as described in §2.1, except for NGC 5194, which is from Tully (1974); Col. (6) Galaxy position angle, measured positive from North to East, in the K_s band (Jarrett et al. 2000, 2003), as described in §2.1; Col. (7) Surface. Col. (8) Nebular reddening determined from the observed Hα/Hβ ratio (Moustakas & Kennicutt 2006), assuming an intrinsic ratio of 2.86 and the O'Donnell (1994) Milky Way extinction curve; Oxygen abundances have been computed using the observed line fluxes [Cols. (9) and (12)], the reddening-corrected line fluxes [Cols. (10) and (13)], and the emission-line equivalent widths (EWs) [Cols. (11) and (14)].

[a]Oxygen abundances derived using either the McGaugh (1991, M91) or the Pilyugin & Thuan (2005, PT05) abundance calibrations. See §3.1 for details.

TABLE 2
H II-Region Oxygen Abundance Gradients

Galaxy (1)	M91[a] 12+log(O/H) at $\rho = 0$ (2)	M91[a] 12+log(O/H) at $\rho = 0.4\,\rho_{25}$ (3)	M91[a] Gradient (dex ρ_{25}^{-1}) (4)	PT05[a] 12+log(O/H) at $\rho = 0$ (5)	PT05[a] 12+log(O/H) at $\rho = 0.4\,\rho_{25}$ (6)	PT05[a] Gradient (dex ρ_{25}^{-1}) (7)	N(H II) (8)	Refs. (9)
NGC 1058	9.09 ± 0.01	8.93 ± 0.01	-0.41 ± 0.02	8.37 ± 0.02	8.35 ± 0.01	-0.05 ± 0.03	6	1
NGC 2541	8.46 ± 0.08	8.51 ± 0.04	0.13 ± 0.17	8.15 ± 0.19	8.21 ± 0.08	0.16 ± 0.41	19	2
NGC 2903	9.11 ± 0.01	8.90 ± 0.01	-0.54 ± 0.03	8.56 ± 0.03	8.37 ± 0.01	-0.46 ± 0.07	45	2,3,4,5
NGC 3198	8.98 ± 0.07	8.72 ± 0.03	-0.65 ± 0.13	8.54 ± 0.16	8.32 ± 0.07	-0.54 ± 0.30	14	2
NGC 3344	9.09 ± 0.05	8.76 ± 0.02	-0.82 ± 0.11	8.34 ± 0.10	8.28 ± 0.04	-0.16 ± 0.22	15	2,4,6
NGC 3351	9.17 ± 0.01	9.09 ± 0.01	-0.21 ± 0.02	8.68 ± 0.16	8.60 ± 0.07	-0.21 ± 0.22	14	4,7,8
NGC 3521	9.17 ± 0.06	8.83 ± 0.03	-0.84 ± 0.20	8.41 ± 0.14	8.36 ± 0.07	-0.11 ± 0.50	12	2,7
NGC 4254	9.18 ± 0.01	8.99 ± 0.01	-0.47 ± 0.03	8.62 ± 0.05	8.46 ± 0.02	-0.40 ± 0.07	18	4,9,10
NGC 4303	9.17 ± 0.02	8.87 ± 0.01	-0.76 ± 0.05	8.52 ± 0.05	8.36 ± 0.02	-0.40 ± 0.10	22	10,11
NGC 4321	9.26 ± 0.03	9.06 ± 0.01	-0.48 ± 0.07	8.67 ± 0.11	8.50 ± 0.04	-0.42 ± 0.19	9	4,10
NGC 4651	8.94 ± 0.01	8.81 ± 0.01	-0.32 ± 0.03	8.37 ± 0.04	8.32 ± 0.02	-0.13 ± 0.05	7	12
NGC 4713	9.03 ± 0.05	8.73 ± 0.01	-0.76 ± 0.10	8.55 ± 0.08	8.33 ± 0.02	-0.55 ± 0.17	4	12
NGC 4736	8.91 ± 0.01	8.85 ± 0.01	-0.17 ± 0.06	8.44 ± 0.03	8.31 ± 0.04	-0.31 ± 0.17	15	4,7,8
NGC 5194	9.20 ± 0.01	9.04 ± 0.00	-0.41 ± 0.03	8.67 ± 0.04	8.54 ± 0.01	-0.33 ± 0.08	34	4,7,13,14,15

References. — (1) Ferguson et al. (1998); (2) Zaritsky et al. (1994); (3) Bresolin et al. (2005); (4) McCall et al. (1985); (5) van Zee et al. (1998); (6) Vilchez et al. (1988); (7) Bresolin et al. (1999); (8) Oey & Kennicutt (1993); (9) Henry et al. (1994); (10) Shields et al. (1991); (11) Henry et al. (1992); (12) Skillman et al. (1996); (13) Bresolin et al. (2004); (14) Diaz et al. (1991); (15) Garnett et al. (2004).

Note. — Col. (1) Galaxy name; Cols. (2) and (5) Central abundance (at radius $\rho = 0$) based on the derived abundance gradient; Cols. (3) and (6) *Characteristic* abundance (at $\rho = 0.4\rho_{25}$), based on the derived abundance gradient; Cols. (4) and (7) Slope of the abundance gradient; Col. (8) Number of H II regions; Col. (9) H II-region references.

[a]Oxygen abundances and abundance gradients derived using either the McGaugh (1991, M91) or the Pilyugin & Thuan (2005, PT05) abundance calibrations. See §3.1 for details.

TABLE 3
Integrated vs. Characteristic Abundance Residuals

Method[a]	M91[b] $\langle\Delta\log(O/H)\rangle$	M91[b] $\Delta\log(O/H)_{median}$	PT05[b] $\langle\Delta\log(O/H)\rangle$	PT05[b] $\Delta\log(O/H)_{median}$
Observed	0.049 ± 0.055	0.047	0.085 ± 0.083	0.093
Corrected	-0.003 ± 0.063	-0.008	-0.028 ± 0.093	-0.009
EWs	-0.063 ± 0.088	-0.042	-0.111 ± 0.128	-0.087

[a]Integrated abundances based on the observed emission-line fluxes, the reddening-corrected line-fluxes, or the emission-line equivalent widths (EWs). See §3.1 for details.

[b]Oxygen abundances derived using either the McGaugh (1991, M91) or the Pilyugin & Thuan (2005, PT05) abundance calibrations. See §3.1 for details.

TABLE 4
Residual Correlation Coefficients[a]

Variables	M91[b] Coefficient	M91[b] Probability	PT05[b] Coefficient	PT05[b] Probability
$\Delta\log(O/H)_{obs}$ vs. Slope	-0.26	0.42	-0.07	0.83
$\Delta\log(O/H)_{obs}$ vs. $E(B-V)$	0.08	0.81	0.31	0.33
$\Delta\log(O/H)_{obs}$ vs. i	0.42	0.17	0.22	0.50
$\Delta\log(O/H)_{obs}$ vs. $\Sigma(H\alpha)$	-0.39	0.21	-0.14	0.66
$\Delta\log(O/H)_{cor}$ vs. Slope	-0.22	0.50	0.16	0.62
$\Delta\log(O/H)_{cor}$ vs. $E(B-V)$	-0.10	0.76	-0.13	0.70
$\Delta\log(O/H)_{cor}$ vs. i	0.37	0.24	0.04	0.90
$\Delta\log(O/H)_{cor}$ vs. $\Sigma(H\alpha)$	-0.41	0.18	-0.20	0.54
$\Delta\log(O/H)_{EW}$ vs. Slope	-0.29	0.35	-0.13	0.68
$\Delta\log(O/H)_{EW}$ vs. $E(B-V)$	-0.02	0.95	0.19	0.56
$\Delta\log(O/H)_{EW}$ vs. i	0.27	0.39	0.16	0.62
$\Delta\log(O/H)_{EW}$ vs. $\Sigma(H\alpha)$	-0.11	0.73	0.15	0.65

[a]Spearman rank correlation coefficients and the probability that the variables are *uncorrelated*. We compare the residuals, $\Delta\log(O/H)$, for all three integrated abundance measurements (see §3.1 for details), against the slope of the abundance gradient, the dust reddening, $E(B-V)$, the inclination angle, i, and the Hα surface brightness, $\Sigma(H\alpha)$.

[b]Oxygen abundances derived using either the McGaugh (1991, M91) or the Pilyugin & Thuan (2005, PT05) abundance calibrations. See §3.1 for details.